RSC Advances

ROYAL SOCIETY OF CHEMISTRY

www.rsc.org/advances

Journal Name

ARTICLE

Design and Synthesis of Novel Dual-Target Agents for HDAC1 and CK2 Inhibition

HernándezReceived 00th January 20xx,
Accepted 00th January 20xx

DOI: 10.1039/x0xx00000x

www.rsc.org/

M. Purwin,[a,b] J. Hernández-Toribio,[a] C. Coderch,[a] R. Panchuk,[c] N. Skorokhyd,[c] K. Filipiak,[a] B. de Pascual-Teresa, [a]* A. Ramos [a]*

ABSTRACT: Drug entities able to address multiple targets can be more effective than those directed to just one biological target. We disclose herein a series of novel dual inhibitors to target histone deacetylase 1 (HDAC 1) and protein kinase CK2. Our bifunctional compounds combine two complementary chemo-active prototypical scaffolds: a hydroxamate essential for the chelation of the zinc ion present in the active site of HDAC (Zinc Binding Group), and a 4,5,6,7-tetrabromobenzotriazole (TBB) moiety introduced to interact with the ATP binding site in CK2 and to act simultaneously as the cap group in the interaction with HDAC1. The synthesized dual-acting agents exhibited promising inhibitory activities towards HDAC1 and CK2. The best result was obtained for **5c** with an IC_{50} of 5 μM for both enzymes. However, its N-2 substituted isomer **5e** presented the best profile in cell-based assays, with cytotoxic activity in the low micromolar LC_{50} in two mammalian cancer cell lines and 4-fold less activity towards a pseudonormal mammalian cell line. Furthermore, this hybrid molecule induced apoptosis in leukemia cells in a concentration-dependent manner. All together makes **5e** a promising lead compound for future in vivo assays in animal tumor models.

Introduction

Owing to the wide-range importance of chemotherapy as the primary treatment of choice for most cancer cases, the development of new efficient drug entities represents a challenge. To date, significant progress has been made in this area, although most traditional cytotoxic agents are associated with severe toxicities and other undesirable side effects. More recently, combination cancer therapies have expanded the treatment options, including the use of multiple drugs with different pharmacological targets, which can directly achieve the desirable therapeutic outcome concertedly via different mechanisms of action.[1-3] However, the employment of these multi-component drug cocktails can also introduce adverse effects related to pharmacokinetics, unpredictable drug-drug interactions, toxicity and patient incompliance.[4, 5] To address these limitations, an attractive and more elegant strategy in modern cancer medicine is to design a single drug with efficient inhibitory activity for more than one biological target, while maintaining lower side effects.[6-8] In addition, from an efficacy perspective, as well as in terms of cost reduction, the design of multitarget drugs instead of discrete inhibitors is also of increasing interest and prominence.[9, 10] In recent years, the development of dual inhibitors has attracted a great deal of attention among several research groups and successful examples have been published for the treatment of cancer, psychiatric pathologies, inflammation, diabetes and neurodegenerative diseases.[11, 12]

Histone deacetylases (HDACs) are a class of epigenetic enzymes that have generated much interest in cancer therapy, since their aberrant activity has been linked to cell proliferation in a variety of human diseases, most notably myeloid neoplasia and solid tumors.[13-18] These enzymes catalyze the hydrolysis of acetylated lysine side chains in histone and non-histone proteins for transcriptional regulation, cell cycle progression, and apoptosis.[19, 20] There are 18 human HDAC isoforms subdivided into four different classes (I–IV), among which classes I (1, 2, 3 and 8), II (4-7, 9 and 10), and IV (11) are Zn^{2+}-dependent for enzymatic activity. Class I HDACs are ubiquitously expressed and play essential roles in proliferation, while classes II and IV have tissue-specific functions. [21, 22] The maintenance of equilibrium between acetylation and deacetylation of histones and nonhistone substrates is essential for normal cell growth. As a result, the

[a] Departamento de Química y Bioquímica, Facultad de Farmacia, Universidad CEU San Pablo, Urbanización Monteprincipe, 28668, Boadilla del Monte, Madrid, Spain.
[b] Department of Organic Chemistry, The Faculty of Pharmacy with the Division of Laboratory Medicine, Medical University of Bialystok, A. Mickiewicza 2A, 15-222, Bialystok, Poland.
[c] Institute of Cell Biology, NAS of Ukraine, Drahomanov str. 14/16, 79005 Lviv, Ukraine.
*Corresponding authors: For A.R.: phone 34 913724796; e-mail, aramgon@ceu.es. For B. P-T: phone 34 913724777; e-mail, bpaster@ceu.es.
Electronic Supplementary Information (ESI) available: PyMOL representation of the binding of a substrate-like molecule to HDAC-8 as found in 2V5W; the PyMOL representation of the binding of an ATP analog and two bromobenzimiazole derivatives to CK2; the PyMOL representation of the best docking poses of compounds **5a** to **5h** bound to HDAC1 and CK2;, the graphical representation of the number of choline atoms that interact with the vicinity of the Mg^{2+} atom in the CK2 complexes; and the PyMOL superimpositions of the HDAC1 structure obtained with SWISSMODEL and the crystal structure deposited under PDB code: 4BKX. ^{1}H and ^{13}C NMR spectra of compounds **5a-5h**.
See DOI: 10.1039/x0xx00000x

use of HDAC inhibitors (HDACi) as cancer therapeutics has emerged as an area of active investigation. [23, 24] By inducing histone hyperacetylation, these compounds alter gene transcription and can exert antitumor effects through growth arrest, differentiation and/or apoptosis. [25, 26] HDAC inhibition has been consolidated as a strategy in epigenetic drug discovery, with 12 inhibitors currently in clinical trials and the FDA approvals of vorinostat (SAHA)[27] and romidepsin (FK228)[28] for treatment of cutaneous T-cell lymphoma (Figure 1A).

The use of HDACi in combination with other anticancer agents has become a practical method to increase the efficiencies of these agents. There are a few examples of this subtype of bifunctional HDACi derived compounds as therapeutically viable anticancer agents. [29-35] One particularly promising approach is the modulation of receptor tyrosine kinase (RTK) pathways by the action of HDACs inhibitors, leading to potential synergistic effects.[36, 37] In this context, an attractive starting point for a secondary target is protein kinase CK2, which is not only responsible for the regulation of HDACs by post-translational modification (particularly phosphorylation), but also appears to be involved in HDAC activation in hypoxia-associated cancer processes, thus contributing to tumor angiogenesis.[38-40]

CK2 is a ubiquitously expressed, constitutively active and highly conserved protein serine/threonine kinase essential for cell viability, which is composed of tetrameric complexes consisting of two catalytic subunits (CK2α, CK2α') and a dimer of regulatory β subunits. [41, 42] CK2 is a pleiotropic protein kinase with more than 300 substrates, which are localized in different cell compartments and are implicated in various important functions, including gene expression, cell growth and differentiation, signal transduction and apoptosis.[43, 44] It has been recently demonstrated that CK2 plays an important role in many pathologies and abnormal high levels of its enzymatic activity have been found in a large variety of cancer cells.[45] Its proliferative and anti-apoptotic properties create a favourable cellular environment for tumor maintenance and progression, making it a potential target for cancer treatment.[46] Up to date many compounds have been reported as potent CK2 inhibitors.[47, 48] Among the CK2 inhibitors reported so far, ATP-competitive compounds such as coumarin derivatives, ellagic acid, DMAT or TBB stand out for their high efficiency and availability.[49-52] More recently, the benzonaphthyridine derivative CX-4945 has been reported to be a first-in-class, orally bioavailable selective CK2 inhibitor in clinical trials (Figure 1B).[53, 54] Hence, since both CK2 and HDAC are closely related relevant proteins in cancer therapy, we envisioned that concurrent inhibition of these two enzymes, by the design of a novel potential multi-target single molecule, might enhance drug efficacy and overcome the current pharmacokinetic limitations, as well as likely provide beneficial additive or synergistic biological effects. Herein we describe our efforts toward this goal by reporting a new family of dual inhibitors of CK2 and HDAC1. These chimeric compounds contain a TBB moiety as a capping group and a hydroxamic acid as a zinc-binding group (ZBG), which have been linked using a click chemistry approach (Figure 1D).

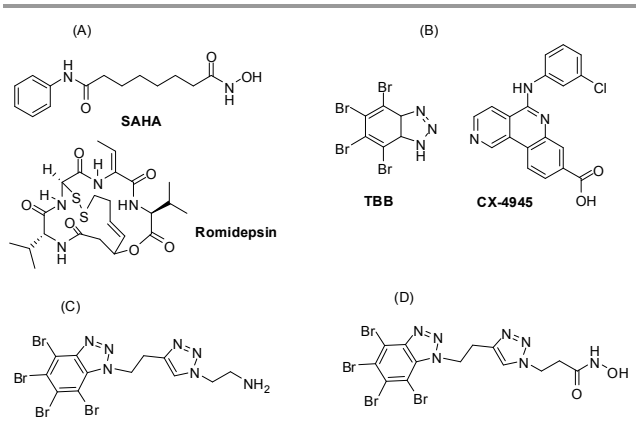

Figure 1. Representative examples of (A) HDAC, (B) CK2 inhibitors, (C) "clicked" CK2 inhibitors, and (D) Chemical structure of one of the designed dual inhibitors.

RESULTS AND DISCUSSION

Design Rationale

HDACis can be broadly described by a common pharmacophore, consisting of a cap group, an appropriate linker and a metal-binding moiety (ZBG), being the latter the primary affinity determinant that coordinates to the active site Zn^{2+} ion (Figure 2A). Among the HDACis, hydroxamic acids exhibit the most potent efficacy since, after ionization, an exceptionally stable 5-membered ring chelate with the active site Zn^{2+} ion is created.

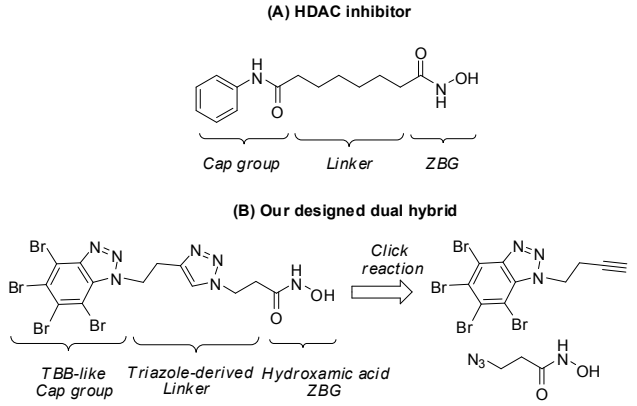

Figure 2. (A) Prototypical structure of HDACi, as exemplified by SAHA. (B) Our click chemistry approach toward bifunctional inhibitors.

We postulated that appropriate conjugation of the surface recognition group (cap) of a prototypical HDACi to other hydrophobic antitumor pharmacophore (e.g., TBB) could furnish the desired bifunctional agents. Presumably, the TBB moiety would act as a surrogate of the cap group in the HDACi and also maintain its activity against the CK2 protein (Figure

2B). This assumption is supported by our previous results,[55] where we described some "clicked" TBB derivatives in which the terminal group is an amino group instead of the hydroxamate present in these new dual-targeting compounds. Those compounds (see Figure 1C) showed Ki values in the low μM range and high degree of selectivity against a panel of 24 kinases.

Chemistry

A series of HDAC-CK2 dual inhibitors has been synthesized. Our approach involves a Cu-catalyzed azide-alkyne 1,3-dipolar cycloaddition (CuAAC)[56] as the crucial step to couple both CK2 and HDAC inhibition scaffolds. As shown in figure 2B, the designed inhibitor has a triazole-alkyl linker, resulting of the click connection of the azide bearing the ZBG and the corresponding TBB-alkyne moiety.

For any synthetic method to be useful, the substrates must be readily accessible. As depicted in scheme 1, alkyne reagents **1** and **2** were prepared by alkylation of TBB with the corresponding alkynyl bromide in the presence of K_2CO_3.[57, 58] While derivative **1** was obtained as a single product after the reaction with propargyl bromide, the presence of an extra carbon in the bromide reagent resulted in the formation of both *N*-1 (**2a**) and *N*-2 (**2b**) alkylated isomers. Fortunately, they were successfully isolated by column chromatography and further tested separately to evaluate the influence of the *N*-substitution pattern in the inhibitor structure.

Likewise, azides with the hydroxamate function were easily obtained in two steps from the corresponding bromo-derived carboxylic acids (Scheme 2). Thus, the synthesis of the intermediates **3a-d** was accomplished by standard azide formation starting from the corresponding bromide. Further reaction of the acid group with *O*-THP hydroxylamine by EDC coupling led to the desired aliphatic and aromatic azides **4a-d**.

Scheme 1[a]

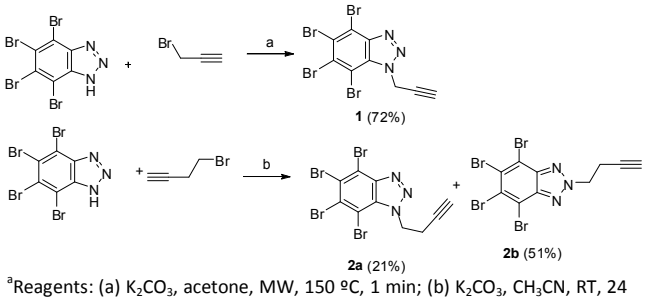

[a]Reagents: (a) K_2CO_3, acetone, MW, 150 ºC, 1 min; (b) K_2CO_3, CH_3CN, RT, 24 h

To examine the effect of the linker length on both sides of the triazole ring, TBB derivatives **1** and **2a-b** as well as azides **4a-c** were selected for the click reaction.

The CuAAC reaction is a regioselective process, forming exclusively the 1,4-substituted adduct.[59] Accordingly, we found that only one isomer was obtained, thus achieving the triazole-based conjugates in excellent yields (Scheme 3). We identified

Scheme 2[a]

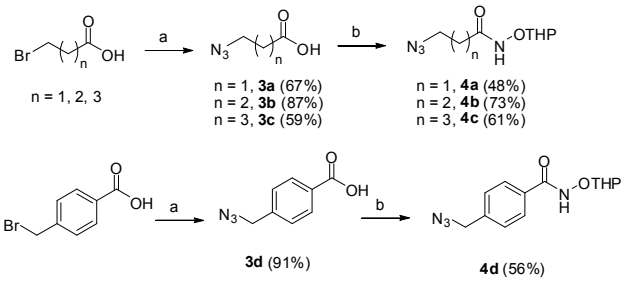

[a]Reagents: (a) NaN_3, DMF, 60 ºC, 12h; (b) NH_2OTHP, HOBt, EDCI, NMM, DMF, rt, 12 h

the use of $CuSO_4$/Na-ascorbate catalytic system and DMF as the optimized conditions for the cycloaddition step. Subsequent removal of the THP protecting group furnished the final hydroxamic acid-based dual inhibitors **5a-f.**

The influence of the position of the attachment (*N*-1 or *N*-2) of the linker to the TBB moiety was analyzed by preparing a representative set of *N*-1 and *N*-2 alkyl derivatives (**5a-f**).

Compounds **5g-h** were selected to study the influence of the introduction of an aromatic ring attached to the hydroxamate group on the inhibition of the target proteins.

Scheme 3[a]

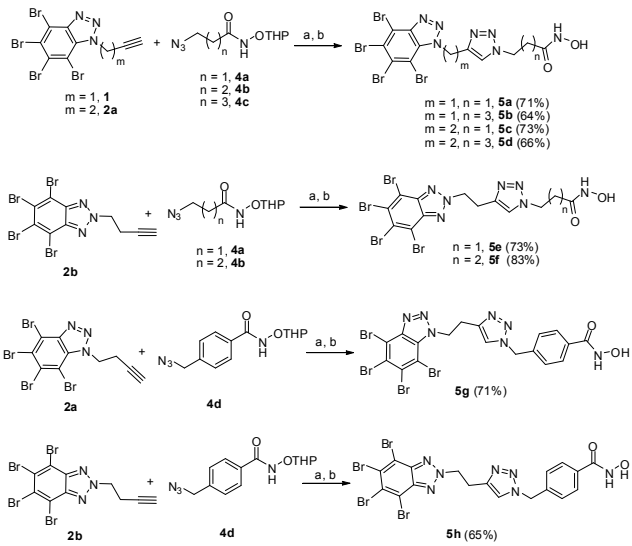

[a]Reagents: (a) $CuSO_4$ (10 mol%), Na-Ascorbate (30 mol%), DMF, rt, 24 h; (b) 4N HCl in dioxane, MeOH, rt, 2h.

Biological evaluation

The inhibitory activities of the synthesized compounds were determined against both enzymes CK2 and HDAC1. The percentage of inhibition at 50 μM concentration of the tested

compound is collected in table 1. The IC_{50} for those compounds showing an inhibition higher than 75% was calculated, and the values are depicted also in table 1.

Table 1. Percentage of inhibition of **5a-h** for CK2α and HDAC1 at 50 μM. (IC_{50} for compounds with an inhibition higher than 75% at 50 μM)

Compound	% Inhibition CK2α, 50 μM (IC_{50}, μM)[a]	% Inhibition HDAC1, 50 μM (IC_{50}, μM)[a]
5a	22.7	32.2
5b	42.0	3.5
5c	79.0 (5.4±1.2)	90.0 (5.0±1.8)
5d	61.2	65.2
5e	61.6	97.0 (2.2±0.2)
5f	47.7	88.3 (5.1±2.4)
5g	47.2	99.0 (1.6±0.4)
5h	22.2	86.0 (2.9±1.1)
TBB	99.8(0.8±0.1)	-
SAHA	-	25.8 (at 0,1 μM)

[a] Enzymatic data are mean values from at least two independent experiments ±SD.

The activity towards human recombinant HDAC1 was tested using a fluorimetric substrate. Compounds **5c, 5e** and **5f** presented the highest potency within the compounds with aliphatic linkers, with IC_{50} of 5.0 ± 1.8 μM, 2.2 ± 0.2 μM and 5.1 ± 2.4 μM respectively (inhibitory activities between 88 and 97% at 50 μM) while **5d** inhibited the deacetylase activity at a lower extent (65.2% at 50 μM) and weak or no inhibition was observed for compounds **5a** and **5b** in the same conditions.

The introduction of an aromatic ring in the linker was beneficial for the inhibition of HDAC1, and **5g** displayed the highest HDAC1 inhibition of all tested compounds with an IC_{50} of 1.6 ± 1.1 μM.

The inhibitory activities of these compounds for CK2 were measured using a radiometric method with a short peptide (RRRADDSDDDDD) as a substrate. Recombinant human CK2α was used as a source of CK2. The best potency against CKα was found for compound **5c** (79% of inhibition at 50 μM, IC_{50} of 5.4 ± 1.2 μM,), which bears the linker attached to the N-1 position of TBB and two CH_2 groups connecting the triazole ring to both TBB and the ZBG. The distance between TBB and the triazole ring provided by a 2(CH_2) linker seems to be crucial for activity. Thus, compounds **5a** and **5b**, where only one methylene group is present at this position are weaker inhibitors (22.7% of inhibition for **5a**; 42% for **5b**). However, more than 60% of inhibition at 50 μM was maintained for compound **5d,** which differ from **5b** in the presence of one additional CH_2 group at this position.

The effect of changing the position of attachment of the alkyl linkers to the N-2 position of TBB was examined through compounds **5e**-**f**. Again the best activity was obtained for the compound bearing 2(CH_2) linkers at both sides of the connecting triazole (compound **5e**, 61.6% of inhibition at 50 μM), while an increase in the number of CH_2 groups, such as in **5f** brought about a loss of activity.

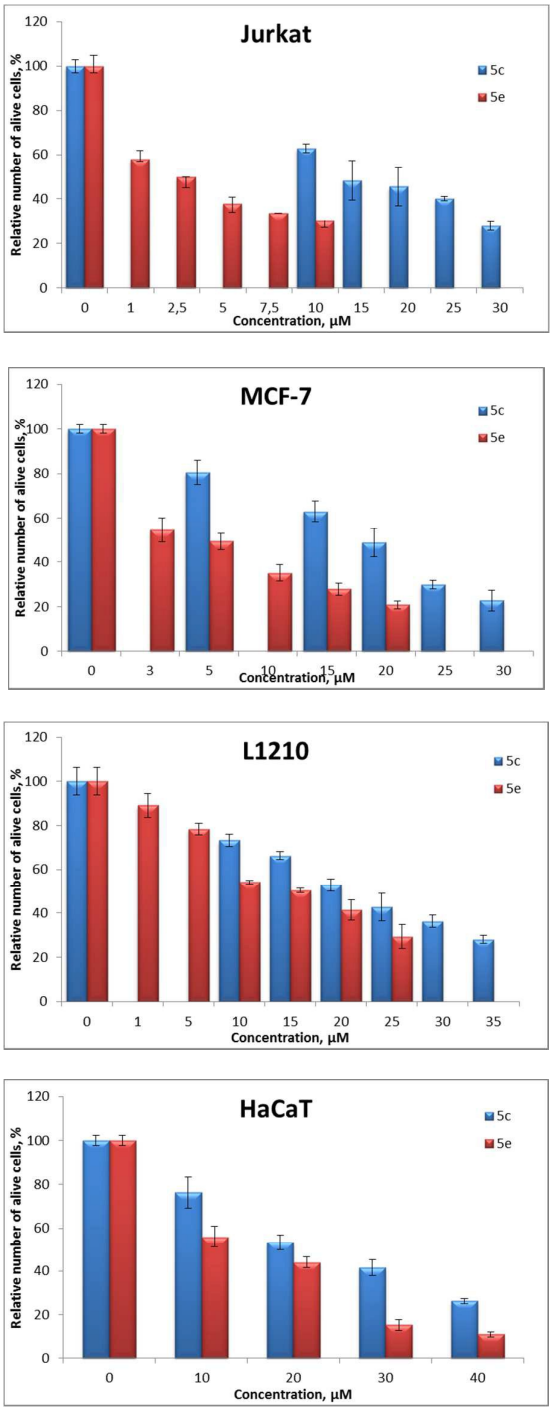

Figure 3. Cytotoxic effect of dual CK2/HDAC inhibitors **5c** and **5e** towards human T-leukemia cells of Jurkat line, human breast adenocarcinoma cells of MCF-7 line, murine leukemia cells of L1210 line, and human immortalized keratinocytes of HaCat line, after 24 h of incubation

To study the influence of the introduction of an aromatic ring in the linker, compounds **5g-h** were synthesized. Both compounds showed a significant loss of activity (47.2% of

inhibition for **5g** and 22.2% of inhibition for **5h**) when compared to its non-aromatic analogues **5d** and **5f** of similar chain length. This loss of activity is probably due to an increase on the rigidity of the molecule.

In summary, the described compounds have a potential interest as dual target inhibitors, and compound **5c** presents the best profile, with identical IC_{50} values in the low micromolar range for CK2 and HDAC1. Therefore, it was selected to evaluate its antiproliferative effect on several cancer cell lines, and proapoptotic activity towards human Jurkat T-leukemia and MCF-7 breast adenocarcinoma. We selected also compound **5e** as representative of the N-2 substituted derivatives.

Cytotoxic activity of the selected inhibitors was evaluated in vitro and the LC_{50} index, calculated as concentration of drug which kills 50% cells in comparison to control, was used to express the effective inhibition. Both compounds exhibited cytotoxic activity in the micromolar range towards several mammalian tumor cell lines (Figure 3).

Interestingly, **5e** showed 1.6-4.7 fold higher activities compared to its isomer **5c**. Human leukemia cells of Jurkat line (LC_{50}=2.9 μM) and human breast adenocarcinoma cells of MCF-7 line (LC_{50}=4.26 μM) were the most sensitive to **5e** action, while human immortalized keratinocytes of HaCat cells were found to be 3-fold more resistant to this compound (LC_{50}=13.66 μM), indicating a selectivity of action of this dual CK2/HDAC inhibitor towards tumor cells. Its isomeric compound **5c** demonstrated weaker cytotoxic activity towards all studied cell lines (LC_{50} in the range of 13.59-27.81 μM), and lack of selectivity for tumor against pseudonormal mammalian cell lines (Table 2).

Table 2. Comparison of LC_{50} values of dual CK2/HDAC inhibitors **5c** and **5e** towards several mammalian cell lines

Cell line	Origin	**5c**, LC_{50}, μM	**5e**, LC_{50}, μM	**5c:5e**
Jurkat	Human leukemia	13.59±1.04	2.87±1.14	4.74
L1210	Murine leukemia	20.90±1.03	13.09±1.07	1.60
MCF-7	Human breast adenocarcinoma	17.27±1.07	4.26±1.09	4.05
293T	Human embryonic kidney cells, transfected by SV40 virus	27.81±1.05	14.55±1.11	1.91
HaCat	Human immortalized keratinocytes	22.06±1.05	13.66±1.08	1.61

Three main cell death mechanisms have been identified – apoptosis, autophagy, and necrosis.[60] Cell necrosis is an undesirable phenomenon during chemotherapy treatment, since it results in the development of massive inflammatory processes in the organism of cancer patients which can significantly complicate the treatment process. By contrast, the induction of apoptosis by anticancer drugs leads to quick phagocytosis of remnants of tumor cells by the macrophages which considerably diminish the development of side effects of chemotherapy.

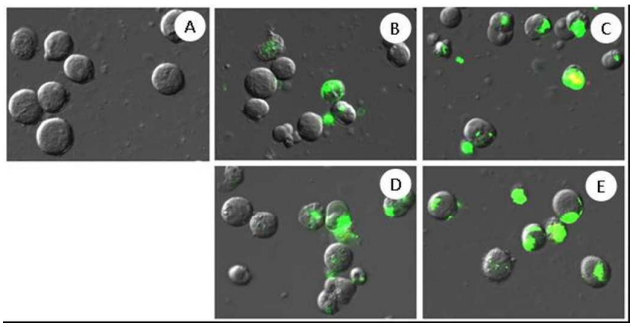

Figure 4. Proapoptotic activity of dual CK2/HDAC inhibitors (Jurkat T-leukemia cells, combined annexin V/PI staining, 24h). A) Control, B) 5c (15 μM), C) 5c (30 μM), D) 5f (3 μM), E) 5f (10 μM). Green color – FITC-conjugated annexin V, orange color – propidium iodide.

Cytomorphologic studies were performed to identify by which way – apoptotic or necrotic – our dual CK2-HDAC inhibitors induced the death of target cells. Phosphatydylserine translocation to the external layer of the cell membrane of dying cells, measured by the Annexin V test, is considered one of the earliest hallmarks of apoptosis.[61] Propidium iodide is a DNA targeting dye which detects only necrotic cells, since alive cells use membrane pumps to move it out to the extracellular medium. Supravital double staining with FITC-conjugated Annexin V and propidium iodide of Jurkat T-leukemia cells treated with **5c** and **5e** in LC_{50} and LC_{75} doses, revealed that both compounds induced apoptosis in leukemia cells (Fig. 4). It should be stressed that the rate and intensity of apoptosis under the action of these novel dual CK2/HDAC inhibitors increased in a concentration-dependent manner. In particular, the treatment at LC_{75} concentration led to a proportional increase in the number of annexin V positive, PI-negative (early apoptotic cells) compared to their action at LC_{50} (Figure 4). On the other hand, inhibitor **5e** led to induction of apoptosis at lower concentration (3 μM for LC_{50} and 10 μM for LC_{75}) than **5c,** which was able to induce appearance of comparable percent of annexin V+/PI- cells only at significantly higher concentrations (15 μM for LC_{50} and 30 μM for LC_{75}, respectively). This result is in accordance with the higher cytotoxic activity displayed by **5e** in this tumor cell line. Cytotoxic and proapoptotic activities of **5c** and **5e** were compared to the ones of TBB and SAHA in human Jurkat T-leukemia cells (Suppl. Fig. S1). Interestingly **5e** possesses significantly higher activity (LC_{50}=2,5 μM) than TBB (LC_{50}=20 μM) and, although LC_{50} of **5e** is identical to that of SAHA, its proapoptotic activity is significantly higher, as revealed by quantitative annexin V/PI assay by flow cytometry. Thus, dual CK2-HDA1C inhibitor **5e** demonstrated an improved behavior in cell-based antitumor assays compared to its predecessors TBB and SAHA, demonstrating the interest of this type of dual targeting inhibitors.

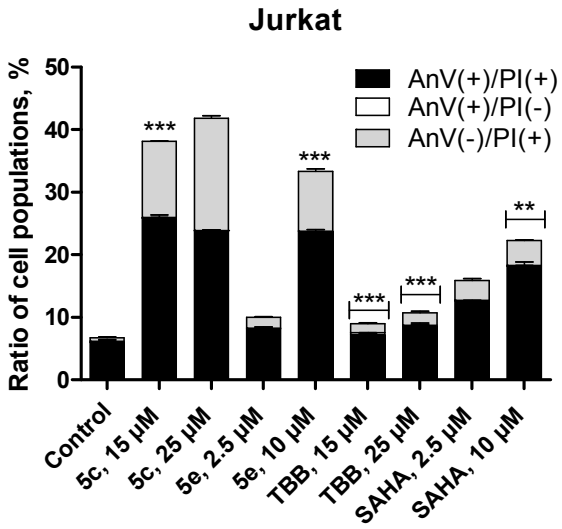

Figure 5. Comparison of proapoptotic activity of compounds **5c, 5e**, TBB and SAHA towards human Jurkat T-leukemia cells. After a 24 h exposure cells were stained with FITC-Annexin V and PI for further analysis by flow cytometry. ***p < 0.001 relative to control, unpaired t-test, ** p < 0.01 relative to 5e, 10 μM, unpaired t-test, ** p < 0.001 relative to 5e, 10 μM, unpaired t-test.

Quantitative annexin V/PI assay by flow cytometry showed that both **5c** and **5e** in sub-LC_{75} doses (15-25 μM for **5c** and 10 μM for **5e**) led to significant and almost identical increase (24-25%) in population of late apoptotic cells (AnV (+)/PI (+)). However, cell treatment with **5c** was accompanied by the appearance of a higher number of necrotic cells (12-18% AnV (-)/ PI(+)) compared to **5e** (9.5%), and the same dependency was also observed in previous experiment (see Figure 4). Thus, **5e** induces mostly late apoptosis in Jurkat T-leukemia cells, while **5c**, besides having weaker cytotoxic activity, is inducing both necrosis and late apoptosis in these cells, which is considered harmful on the physiological level. Surprisingly, both **5c** and **5e** demonstrated much higher proapoptotic activity compared to TBB (8,5% late apoptotic cells) and SAHA (18% late apoptotic cells), also taken in sub-LC_{75} concentrations (Figure 5). These results clearly demonstrate better propoapoptotic activities of novel hybrid CK2-HDAC1 inhibitors compared to their parental compounds.

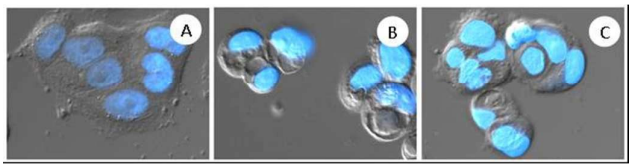

Figure 6. Cytomorphological studies of chromatin structure of MCF-7 cells under treatment with dual CK2/HDAC inhibitors. DAPI staining, 24 h. A) Control, B) **5c** (25 μM), C) **5e** (10 μM)

Nuclear chromatine hypercondensation is considered to be another typical hallmark of apoptosis. It can be easily measured by using DNA-intercalating dyes, such as DAPI (4',6-diamidino-2-phenylindole). Both **5c** and **5e** led to chromatine hypercondensation, vacuolization of cytosol and formation of membrane blebs at 25 μM and 10 μM concentrations (Figure 6), which correspond to apoptosis induction. These results fully confirm the annexin V/PI data.

Computational Studies

In order to give a rationale for the results shown in Table 1, the predicted binding-mode of the described compounds to both enzymes was studied by means of molecular modeling techniques.

HDAC1 binding. The catalytic site of HDAC1 is located at the centre of the enzyme and is accessed through a small hydrophobic tunnel. The side chains of Phe150 and Phe205 leave a gap of approximately 8 Å between them making up this tunnel, at the bottom of which lays the catalytic Zn^{2+} ion. In normal conditions, the acetylated Lys of the substrate plunges into the tunnel reaching the Zn^{2+} and becomes part of the coordination sphere through the carbonyl oxygen, which catalyses the deacetylation reaction with the participation of a water molecule, as can be seen in the crystal structure of HDAC8 in complex with a substrate-like molecule (Supplementary Figure S1).[62] HDAC inhibitors carrying a ZBG target the enzyme by chelating the Zn^{2+} and becoming part of its coordination sphere, while the linker interacts with the walls of the tunnel and the capping moiety protrudes out of it and interacts with the surface of the protein.[63, 64] Crystallographic studies have shown that hydroxamic acid-bearing inhibitors establish a hydrogen bonding network between conserved His residues in the active site and coordinate Zn^{2+} in a bidentate way, replacing the active-site water molecule with one of the oxygen atoms.[62] Moreover, computational studies suggested that one of the His residues in the binding site could be protonated as part of the deacetylation reaction mechanism.[65] In this same line, the binding poses obtained for the set of our newly synthesized inhibitors buried the hydroxamic acid moiety deep into the active site, coordinating the two oxygen atoms with the catalytic Zn^{2+} ion. Apart from chelating the Zn^{2+}, the hydroxamic moiety established several hydrogen bond interactions, and we observed that the terminal OH could be easily deprotonated by the imidaloze side chain of His140. Therefore the dockings and further calculations were carried out with the deprotonated hydroxamates and a protonated side chain of His140. In addition to the hydrogen bond resulting from this deprotonation, the NH group of the hydroxamate interacts with the Nε of the imidaloze side chain of His141, and the carbonyl oxygen with the OH group on the side chain of Tyr303. The linker between the hydroxamate and the triazole can establish van der Waals interactions with Phe150 and Phe205, making the TBB cap protrude out of the binding tunnel. A linker of two or three methylene groups between the hydroxamate and the triazole keep the latter inside the tunnel and at van der Waals interaction reach of the side chains of Phe150 and Phe205 as it's the case for compounds **5a**, **5c** and **5e-f**, whereas **5b** and **5d** that present

four methylene groups make the triazole protrude out of the binding tunnel.

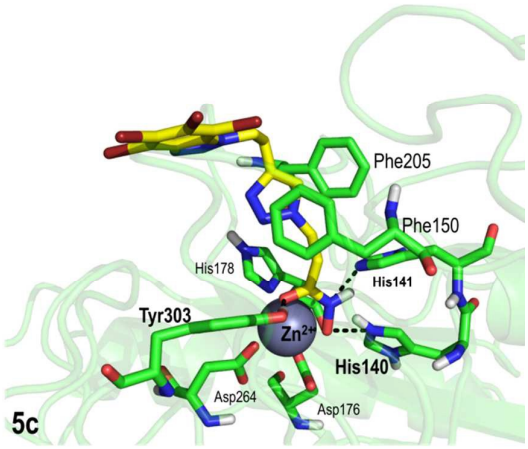

Figure 7: PyMOL stick and semi-transparent cartoon representation of the bound conformation of compounds **5c** and **5e** to HDAC1 after the 10 ns MD simulation. The main amino acids involved in the binding are represented as sticks and the catalytic Zn^{2+} is represented as a grey sphere. Hydrogen bonding and coordinating interactions are shown as dashed lines and the residues involved are labelled in bold. For the sake of clarity only polar hydrogens are shown.

The introduction of an aromatic moiety to the linker between the hydroxamate and the triazole in compounds **5g-h** increases the interaction with the side chains of Phe150 and Phe205 due to the establishment of π-π interactions between the aromatic groups. On the other hand, a shorter linker with only one methylene group between the TBB moiety and the triazole present in compounds **5a** and **5b** reduces the flexibility at the end of the ligand and, therefore, the ability to further accommodate the TBB cap to the surface of the protein outside the tunnel (Supplementary Figure S2).

Given their interesting IC_{50}, the complexes with compounds **5c** and **5e** were subsequently used for MD simulations to further study their binding-stability. In both complexes (Figure 7) the two methylene groups attached to the hydroxamate and the triazole interact with the side chains of Phe150 and Phe205 that make up the walls of the tunnel, while the second two-carbon linker and the TBB moiety protrude out of the binding site and interact with the surface of the protein. During the 10 ns simulation the binding modes of both compounds **5c** and **5e** remained stable and the interactions with the residues in the active site where maintained, while the triazole accommodated itself into the tunnel optimizing the van der Waals contacts with the side chains of Phe150 and Phe205. The different attachment (N1 or N2) of the linker to the TBB moiety does not change much the binding pose outside the catalytic cleft: compound **5c** sits mainly on the side chain of Leu271, whereas compound **5e** sways a little more so it interacts, not only with the side chain of Leu271, but also with Pro29 and with Phe150 in an edge to face interaction with the latter.

CK2 binding. The catalytic subunit of CK2 has the common characteristic structure of all kinases, which is two distinct domains with the ATP binding site between them. This binding site is mainly a hydrophobic flat pocket made up of the side chains of Val53 and Ile66 at the ceiling, and Met163 and Ile174 at the bottom. The natural substrate ATP binds by inserting the adenine into the binding site, thus establishing van der Waals interactions with the amino acids at the bottom and ceiling of the pocket. The position is further stabilized by hydrogen bonding interactions between N1 and N7 of the base and the backbone NH of Val116 and carbonyl of Glu114, respectively; whilst the triphosphate moiety and the two Mg^{2+} ions interact with Asp156, Lys158, Asn161 and Asp175 (Supplementary Figure S3).[66] Albeit having only halogen bond acceptors, TBB is a selective competitive inhibitor of the ATP-binding to CK2. It occupies the ATP-binding pocket establishing strong van der Waals interactions with the side chains of Val53, Ile66, Met163 and Ile174, which due to the shape and size of the pocket they make up, they are responsible for the marked selectivity of TBB for CK2.[67] Moreover, a hydrogen bond between N2 and Lys68 is established, as TBB is deprotonated and negatively charged at physiological pH, as it can be seen in the PDB structure 1J91 (Supplementary Figure S4).[67] In the case of the TBB analogue tetrabromobenzimidazole, the lack of the N2 changes the overall charge of the ligand and thus the ionic interaction with Lys68 is not established. This change modifies the orientation of the binding that promotes the formation of a halogen bond between one of the Br atoms and the backbone carbonyl of Val116 (Supplementary Figure S5).[68] These modifications not only do not impair the binding to CK2, but also make it possible to introduce different substitutions at position 2.

The docking of the majority of the designed inhibitors lodged the TBB moiety in a similar way as in the crystallized complex, burying it deep inside the hydrophobic pocket of CK2 in such an orientation that, in some cases, a halogen bond could be established with the carbonyl oxygen of Val116, similar to the one established by tetrabromobenzoimidazole in PDB code 2OXY. Moreover, in all of these dockings strong van der Waals contacts are established with the side chains of Val45, Val53, Ile66, Val95, Phe113, Val116, Met163 and Ile174, analogue to the ones in the crystallized complexes. Depending on the length of the ligands and the position of the substitution on the TBB moiety they adopt different orientations within the binding site and display different orientations of their substituents. Compounds **5a-5f** orient the hydroxamic acid moiety towards the side chains of Asp156, Lys158, Asn161 and Asp175 that make up one of the Mg^{2+}-binging sites in CK2. The presence of the additional aromatic ring of compounds **5g-h** does not give good binding poses as they are not able to fit within the binding site due to the increase in length derived from the extra aromatic ring and the linker (Supplementary Figure S6). They are not able to interact with the side chains of Asp156, Lys158, Asn161 and Asp175, and due to this increased

length these compounds interact with Val116 through the hydroxamic acid in a bidentate interaction while the TBB moiety sits on top of the side chain of Lys158, probably stabilized by a π-cation interaction. These results suggest that equilibrium between length and ligand flexibility has to be met in order to have an efficient binding of TBB derivatives to the ATP-binding site in CK2. The complexes of CK2 with compound **5c** and its direct analogue **5e**, that presented the highest inhibitory activity, were subjected to MD simulations to further study their binding stability and try to understand the slight differences brought about by distinct TBB substitution.

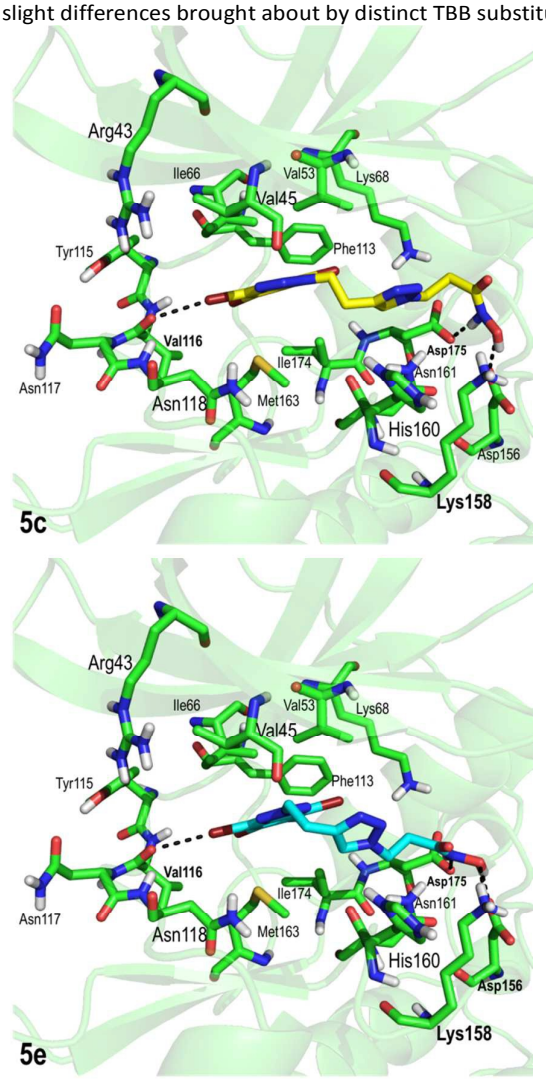

Figure 8: PyMOL stick and semi-transparent cartoon representation of the bound conformation of compounds **5c** and **5e** to CK2 after the 10 ns MD simulation. The main amino acids involved in the binding are represented as sticks. For the sake of clarity only polar hydrogens are shown.

The initial good van der Waals interactions between the TBB moiety of both compounds and the side chains of Val45, Val53, Ile66, Phe113, Met163 and Ile174 (as can be seen in the corresponding images of Supplementary Figure S6) were maintained during the MD simulation, in addition to the interaction of the triazole moiety with the protonated side chain of His160. Both complexes remained quite stable due to the interaction of the hydroxamic acid moiety with the side chains of Asp156, Lys158 and Asp175 and the establishment of a halogen bond between the carbonyl oxygen of the backbone of Val116 and the Br at position 4 and 5 of the TBB moieties of compounds **5e** and **5c**, respectively. (Figure 8).

Experimental

Materials and Methods. Melting points (uncorrected) were taken in open-end capillary tubes and were determined on a Stuart Scientific SMP3 apparatus. Thin-layer chromatography (TLC) was run on Merck silica gel 60 F254 plates. Flash column chromatography was performed using silica gel Merk-60 (230-400 mesh). Unless stated otherwise, purchased starting materials used were high-grade commercial products. NMR spectra were recorded at 400 MHz (1H) and 101 MHz (13C) on a Bruker 400-AC magnetic resonance spectrometer at room temperature in $CDCl_3$ [calibrated at 7.26 ppm (1H) and 77.0 ppm (^{13}C)] and in DMSO-d_6 [calibrated at 2.50 ppm (1H) and 39.5 ppm (^{13}C)]. Data are presented as follows: chemical shift (ppm), multiplicity (s singlet, bs broad singlet, d doublet, t triplet, q quartet, m multiplet), coupling constant *J* (Hz) and integration. Data for ^{13}C NMR are reported in terms of chemical shifts (ppm). HPLC-MS was performed at Synthelia Organics SL., using an Agilent 1100 HPLC system and Xterra C18-5 µm or ACE C18-3µm reverse phase columns. The following conditions were used: method A, Xterra C18-5µm column, a flow rate of 2 mL/min, eluting with solvent A (20 mM NH_4HCO_3/water) and solvent B (ACN) at an isocratic run of 40% of solvent A and 60% of solvent B over 15 min with detection at 254 nm; method B, a flow rate of 0.75 mL/min, eluting with solvent A (20 mM NH_4HCO_3/water) and solvent B (ACN) at a gradient run from 20-95% of solvent B over 6 min with detection at 254 nm. For reporting HPLC-MS data, m/z values and retention time for each method are given. Elemental analyses (C, H, N, S) were performed on a LECO CHNS-932 apparatus at the Microanalyses Service of the Universidad Complutense de Madrid.

4,5,6,7-Tetrabromo-1*H*-benzotriazole (TBB),[69] *N*-alkyl derivatives **1** and **2a-b**[58] and azides **3a-e**[70, 71] were synthesized according to literature procedures. Melting points, ^{1}H and/or ^{13}C NMR data were in agreement with those published.

4,5,6,7-tetrabromo-1-(prop-2-yn-1-yl)-1*H*-benzo[*d*][1,2,3]triazole (1). To a suspension of TBB (500 mg, 1.1 mmol) and K_2CO_3 (1.4 g, 10.15 mmol) in acetone (20 mL) was added 3-bromo-1-propyne (0.3 mL, 3.4 mmol). This reaction was carried out by microwave assistance at 150 °C for 1 min. After cooling to room temperature, the solvent was removed under vacuum and the residue was dissolved in 20 ml of AcOEt and washed with brine (2x20 mL). The organic layer was dried ($MgSO_4$), filtered, evaporated to dryness and purified by flash chromatography (Hex/DCM 4:1) to afford **1** as a white solid (382 mg, 72 %), ^{1}H NMR (400 MHz, DMSO) δ 5.81 (d, *J* = 2.3 Hz, 2H), 3.68 (t, *J* = 2.3 Hz, 1H). ^{13}C NMR (101 MHz,

DMSO) δ 144.8, 131.4, 129.1, 124.1, 115.8, 106.6, 78.3, 77.4, 40.2.

4,5,6,7-tetrabromo-1-(but-3-yn-1-yl)-*1H*-benzo[*d*][1,2,3]triazole (2a) and 4,5,6,7-tetrabromo-2-(but-3-yn-1-yl)-2*H*-benzo[*d*][1,2,3]triazole (2b). To a suspension of TBB (200 mg, 0.46 mmol) and K_2CO_3 (565 mg, 4.1 mmol) in acetonitrile (10 mL) was added 4-bromo-1-butyne (0.12 mL, 1.38 mmol) and the mixture was stirred at RT under argon for 24 hours. After cooling to room temperature, the solvent was removed under vacuum and the residue was dissolved in 20 ml of AcOEt and washed with brine (2x20ml). The organic layer was dried ($MgSO_4$), filtered, evaporated to dryness and purified by flash chromatography (Hex/DCM 4:1) to afford **2a** (47 mg, 21%) and **2b** (114 mg, 51%). **2a**: ^{1}H NMR (400 MHz, DMSO) δ 5.07 (t, *J* = 6.8 Hz, 2H), 2.96-2.86 (m, 3H). ^{13}C NMR (101 MHz, DMSO) δ 144.8, 131.8, 128.7, 123.6, 115.8, 106.9, 79.7, 74.0, 48.1, 20.5. **2b**: ^{1}H NMR (400 MHz, DMSO) δ 4.94 (t, *J* = 6.7 Hz, 2H), 3.03 (td, *J* = 6.7, 2.6 Hz, 2H), 2.87 (t, *J* = 2.6 Hz, 1H). ^{13}C NMR (101 MHz, DMSO) δ 142.5, 125.8, 113.6, 79.8, 73.6, 55.5, 19.1.

General procedure for the synthesis of azides 3a-d. To a solution of the corresponding alkyl bromide (1.0 mmol) in DMF (5 mL) under argon was added NaN_3 (65 mg, 1.0 mmol) and the mixture was stirred at 60 ºC overnight. After cooling to room temperature, AcOEt (20 mL) and aqueous HCl 0.1 M (20 mL) were successively added, and the water phase was extracted with AcOEt (2 x 20 mL). The combined organic extracts were washed with brine, dried over $MgSO_4$, filtered and concentrated under vacuum to afford the desired azides, which were used in the next step without further purification.

3-azidopropanoic acid (3a). Following the general procedure, the reaction of 3-bromopropionic acid (1.0 g, 6.5 mmol) with NaN_3 (423 mg, 6.5 mmol) gave **3a** as a white solid (501 mg, 67%). ^{1}H NMR (400 MHz, $CDCl_3$) δ 3.58 (t, *J* = 6.4 Hz, 2H), 2.62 (t, *J* = 6.4 Hz, 2H).

4-azidobutanoic acid (3b). The reaction of 4-bromobutanoic acid (835 mg, 5 mmol) with NaN_3 (325 mg, 5 mmol) gave **3b** as a white solid (561 mg, 87%). ^{1}H NMR (400 MHz, $CDCl_3$) δ 3.38 (t, *J* = 7.2 Hz, 2H), 2.26 (t, *J* = 7.2 Hz, 2H), 1.97-1.88 (m, 2H).

5-azidopentanoic acid (3c). The reaction of 5-bromopentanoic acid (1.0 g, 5.5 mmol) with NaN_3 (358 mg, 5.5 mmol) gave **3c** as a white solid (464 mg, 59%). ^{1}H NMR ($CDCl_3$, 400 MHz) δ 3.26-3.33(m, 2H), 2.36-2.42 (m, 2H), 1.60-1.75 (m, 4H).

4-(azidomethyl)benzoic acid (3d). The reaction of 4-(bromomethyl)benzoic acid (1.0 g, 4.7 mmol) with NaN_3 (306 mg, 4.7 mmol) gave **3d** as a white solid (752 mg, 91%). ^{1}H NMR (400 MHz, $CDCl_3$) δ 8.12 (s, 1H), 7.50-7.38 (m, 4H), 2.48 (s, 2H).

4-azidobenzoic acid (3e). To a solution of methyl 4-aminobenzoate (1.0 g, 6.6 mmol) in anhydrous CH_3CN (60 mL) under argon were successively added *t*-BuONO (1.3 mL, 9.9 mmol) and $TMSN_3$ (1.0 mL, 7.9 mmol) dropwise at 0 °C. The reaction mixture was stirred at the same temperature for 30 min and at room temperature for 3 h. The solvent was removed under vacuum and the residue was purified by flash chromatography (Hexane/AcOEt 95:5) to afford 640 mg of a white solid, which was subsequently dissolved in methanol (3 mL). To this solution, aqueous NaOH 1M (3 mL) was added and the mixture was stirred for 2 h at room temperature. After addition of AcOEt (10 mL) the solution was neutralized with aqueous HCl 1M (pH ≈ 1). The two phases were separated and the water phase was extracted with AcOEt (2 x 10 mL). The combined organic extracts were washed with brine, dried over $MgSO_4$ and concentrated under vacuum to give **3e** as a white solid (570 mg, 53% over two steps). ^{1}H NMR (400 MHz, $CDCl_3$) δ 8.10 (d, *J* = 8.5 Hz, 2H), 7.11 (d, *J* = 8.5 Hz, 2H).

General procedure for the synthesis of hydroxamate derivatives 4a-e. To a solution of the corresponding acid (**3a-e**) (2.0 mmol) in DMF (10 mL) were successively added HOBt (1.2 equiv, 324 mg, 2.4 mmol), NMM (3 equiv, 0.66 mL, 6.0 mmol), NH_2OTHP (2 equiv, 468 mg, 4.0 mmol) and EDCI (1.4 equiv, 538 mg, 2.8 mmol) and the mixture was stirred at room temperature overnight. The solution was then diluted with AcOEt (40 mL) and subsequently washed with saturated aqueous NH_4Cl (40 mL) and brine, dried over $MgSO_4$. The drying agent was filtered off, the solvent was removed in vacuo and the residue was purified by flash chromatography on silica gel (the eluent is indicated in each case) to afford the desired hydroxamic acid derivatives **4a-e**.

3-azido-*N*-((tetrahydro-2*H*-pyran-2-yl)oxy)propanamide (4a). Following the general procedure, the reaction of 3-azidopropanoic acid **3a** (230 mg, 2.0 mmol) gave, after flash chromatography (DCM/MeOH 95:5), **4a** as a white solid (205 mg, 48 %). ^{1}H NMR (400 MHz, $CDCl_3$) δ 8.42 (s, 1H), 4.93 (t, *J* = 6.8 Hz, 1H), 3.68-3.52 (m, 2H), 2.33 (t, *J* = 6.9 Hz, 2H), 1.77 (t, *J* = 6.8 Hz, 2H), 1.69-1.47 (m, 6H).

4-azido-*N*-((tetrahydro-2*H*-pyran-2-yl)oxy)butanamide (4b). Following the general procedure, the reaction of 4-azidobutanoic acid **3b** (258 mg, 2.0 mmol) gave, after flash chromatography (Hexane/AcOEt 3:2), **4b** as a white solid (333 mg, 73 %). ^{1}H NMR (400 MHz, $CDCl_3$) δ 8.36 (s, 1H), 4.96 (t, *J* = 7.0 Hz, 1H), 3.69 (t, *J* = 7.1 Hz, 2H), 2.31-2.24 (m, 2H), 1.99-1.52 (m, 10H).

5-azido-*N*-((tetrahydro-2*H*-pyran-2-yl)oxy)pentanamide (4c). Following the general procedure, the reaction of 5-azidopentanoic acid **3c** (286 mg, 2.0 mmol) gave, after flash chromatography (Hexane/AcOEt 3:2), **4c** as a white solid (295 mg, 61 %). ^{1}H NMR (400 MHz, $CDCl_3$) δ 8.41 (s, 1H), 4.93 (t, *J* = 6.8 Hz, 1H), 3.66-3.58 (m, 2H), 2.39 (t, *J* = 6.9 Hz, 2H), 1.97 - 1.55 (m, 12H).

4-(azidomethyl)-*N*-((tetrahydro-2*H*-pyran-2-yl)oxy)benzamide (4d). Following the general procedure, the reaction of 4-(azidomethyl)benzoic acid **3d** (354 mg, 2.0 mmol) gave, after flash chromatography (Hexane/AcOEt 7:3), **4d** as a white solid (309 mg, 56 %). ^{1}H NMR (400 MHz, $CDCl_3$) δ 8.98 (s, 1H), 7.77 (d, *J* = 8.1 Hz, 2H), 7.38 (d, *J* = 8.1 Hz, 2H), 5.07 (t, *J* = 6.8 Hz, 1H), 4.39 (s, 2H), 4.05-3.93 (m, 1H), 3.72-3.52 (m, 1H), 1.85-1.52 (m, 6H).

4-azido-*N*-((tetrahydro-2*H*-pyran-2-yl)oxy)benzamide (4e). Following the general procedure, the reaction of 4-azidobenzoic acid **3e** (326 mg, 2.0 mmol) gave, after flash chromatography (DCM/MeOH 9:1), **4e** as a white solid (309 mg, 59 %). ^{1}H NMR (400 MHz, DMSO) δ 9,02 (s, 1H), 7.82 (d, *J* = 7.6 Hz, 2H), 7.40 (d, *J* = 7.6 Hz, 2H), 4,98 (t, *J* = 7.2 Hz, 1H), 3,52 (t, *J* = 7.1 Hz, 2H), 1.86-1.48 (m, *J* = 7.1 Hz, 6H).

General procedure for the click reaction: synthesis of triazole-based dual inhibitors 5a-h. To a mixture of the azide (0.1 mmol) and the corresponding alkyne (1.1 equiv, 0.11 mmol) in DMF (1 mL) under argon, were successively added sodium ascorbate (30 mol%, 0.03 mmol, 30 µL of freshly prepared 1M solution in water) and copper (II) sulfate pentahydrate (10 mol%, 0.01 mmol, 33 µL of freshly prepared 0.3M solution in water). The heterogeneous mixture was stirred vigorously overnight at room temperature. After removing the solvent under vacuum, AcOEt (10 mL) was added and the resulting solution was washed with NH_4Cl (10 mL) and brine and dried over ($MgSO_4$). Filtration and evaporation of the solvent gave a residue which was purified by flash chromatography (the eluent is indicated in each case). Final removal of the THP protecting group was carried out as follows: to a solution of the protected hydroxamic acid in MeOH (4 mL) was added 4M HCl in dioxane (0.4 mL, 0.4 mmol) and the mixture was stirred at room temperature for 2 h. Solvent co-evaporation with MeOH (x 3) afforded the corresponding adducts **5a-h**.

***N*-hydroxy-3-(4-((perbromo-1*H*-benzo[*d*][1,2,3]triazol-1-yl)methyl)-1*H*-1,2,3-triazol-1-yl) propanamide (5a).** Following the general procedure, the reaction of **4a** (30 mg, 0.14 mmol) with **1** (71 mg, 0.15 mmol) afforded, after flash chromatography (Hex/AcOEt 1:3) and further hydroxamate deprotection, **5a** as a white solid (59 mg, 71%), mp 130-132 ºC. ^{1}H NMR (400 MHz, DMSO) δ 10.12 (br s, 1H), 9.93 (br s, 1H), 8.09 (s, 1H), 6.25 (s, 2H), 4.54 (t, *J* = 6.7 Hz, 2H), 2.94 (t, *J* = 6.7 Hz, 2H). ^{13}C NMR (101 MHz, $CDCl_3$) δ 170.8, 145.6, 131.6, 129.80, 124.7, 123.9, 116.8, 114.1, 106.0, 52.3, 46.1, 34.4. HPLC-MS: *m/z* 603 $[M-2H]^+$, t_R: 11.12 min, method A. Anal. calcd for $C_{12}H_{11}Br_4N_7O_2$ requires C, 23.83; H, 1.83; Br, 52.84; N, 16.21; O, 5.29; found: C, 23.72; H, 1.92; N, 16.31.

***N*-hydroxy-5-(4-((perbromo-1*H*-benzo[*d*][1,2,3]triazol-1-yl)methyl)-1*H*-1,2,3-triazol-1-yl)pentanamide (5b).** The reaction of **4c** (30 mg, 0.12 mmol) with **1** (64 mg, 0.14 mmol) afforded, after flash chromatography (Hex/AcOEt 1:5) and further hydroxamate deprotection, **5b** as a white solid (48 mg, 64 %), mp 167-169 ºC. ^{1}H NMR (400 MHz, DMSO) δ 10.04 (br s, 1H), 9.85 (br s, 1H), 8.09 (s, 1H), 6.26 (s, 2H), 4.31 (t, *J* = 7.0 Hz, 2H), 2.30 (t, *J* = 7.4 Hz, 2H), 1.84-1.68 (m, 2H), 1.51-1.37 (m, 2H). ^{13}C NMR (101 MHz, DMSO) δ 172.9, 144.9, 142.0, 131.8, 128.8, 123.7, 123.3, 115.7, 106.8, 51.2, 45.6, 32.4, 28.9, 21.2. HPLC-MS: *m/z* 631 $[M]^+$, t_R: 11.67 min, method A. Anal. calcd for $C_{14}H_{13}Br_4N_7O_2$ requires C, 26.65; H, 2.08; Br, 50.66; N, 15.54; O, 5.07; found: C, 26.49; H, 2.07; N, 15.63.

***N*-hydroxy-3-(4-(2-(perbromo-1*H*-benzo[*d*][1,2,3]triazol-1-yl)ethyl)-1*H*-1,2,3-triazol-1-yl)propanamide (5c).** The reaction of **4a** (30 mg, 0.14 mmol) with **2a** (75 mg, 0.15 mmol) afforded, after flash chromatography (Hex/AcOEt 1:3) and further hydroxamate deprotection, **5c** as a white solid (63 mg, 73%), mp 130-132 ºC. ^{1}H NMR (400 MHz, DMSO) δ 10.50 (br s, 1H), 8.83 (br s, 1H), 7.88 (s, 1H), 5.17 (t, *J* = 7.2 Hz, 2H), 4.51 (t, *J* = 5.3 Hz, 2H), 3.30 (t, *J* = 7.2 Hz, 2H), 2.56 (t, *J* = 5.2 Hz, 2H). ^{13}C NMR (101 MHz, DMSO) δ 165.8, 144.9, 142.0, 131.8, 128.5, 123.5, 123.2, 115.7, 106.8, 49.4, 45.5, 32.7, 27.0. HPLC-MS: *m/z* 618 $[M⍰H]^+$, t_R: 3.01 min, method B. Anal. calcd for $C_{13}H_{11}Br_4N_7O_2$ requires C, 25.31; H, 1.80; Br, 51.81; N, 15.89; O, 5.19; found: C, 25.43; H, 1.75; N, 15.96.

***N*-hydroxy-5-(4-(2-(perbromo-1*H*-benzo[*d*][1,2,3]triazol-1-yl)ethyl)-1*H*-1,2,3-triazol-1-yl)pentanamide (5d).** The reaction of **4c** (25 mg, 0.1 mmol) with **2a** (56 mg, 0.12 mmol) afforded, after flash chromatography (Hex/AcOEt 1:6) and further hydroxamate deprotection, **5d** as a white solid (45 mg, 66%), mp 141-142 ºC. ^{1}H NMR (300 MHz, DMSO) δ 10.19 (br s, 1H), 7.85 (s, 1H), 5.18 (t, *J* = 7.1 Hz, 2H), 4.28 (t, *J* = 6.9 Hz, 2H), 3.32 (t, *J* = 7.1 Hz, 2H), 2.32 (t, *J* = 7.14 Hz, 2H), 1.77-1.69 (m, 2H), 1.46-1.38 (m, 2H). ^{13}C NMR (101 MHz, DMSO) δ 173.0, 144.8, 142.1, 131.8, 128.5, 123.5, 122.9, 115.7, 106.7, 51.2, 49.5, 32.5, 29.0, 27.0. HPLC-MS: *m/z* 645 $[M]^+$, t_R: 3.93 min, method B. Anal. calcd for $C_{15}H_{15}Br_4N_7O_2$ requires C, 27.93; H, 2.34; Br, 49.56; N, 15.20; O,4.96; found: C, 28.50; H, 2.25; N, 14.85.

***N*-hydroxy-3-(4-(2-(perbromo-2*H*-benzo[*d*][1,2,3]triazol-2-yl)ethyl)-1*H*-1,2,3-triazol-1-yl)propanamide (5e).** The reaction of **4a** (30 mg, 0.14 mmol) with **2b** (75 mg, 0.15 mmol) afforded, after flash chromatography (Hex/AcOEt 1:3) and further hydroxamate deprotection, **5e** as a white solid (63 mg, 73%), mp 173-175 ºC. ^{1}H NMR (400 MHz, DMSO) δ 10.48 (br s, 1H), 8.82 (br s, 1H), 7.80 (s, 1H), 5.05 (t, *J* = 7.2 Hz, 2H), 4.49 (t, *J* = 6.7 Hz, 2H), 3.44 (t, *J* = 6.7 Hz, 2H), 2.55 (t, *J* = 7.2 Hz, 2H). ^{13}C NMR (101 MHz, DMSO) δ 165.8, 142.5, 142.2, 125.6, 123.1, 113.6, 56.4, 45.5, 32.7, 25.6. HPLC-MS: *m/z* 618 $[M⍰H]^+$, t_R: 3.34 min, method B. Anal. calcd for $C_{13}H_{11}Br_4N_7O_2$ requires C, 25.31; H, 1.80; Br, 51.81; N, 15.89; O, 5.19; found: C, 25.14; H, 1.75; N, 16.01.

***N*-hydroxy-4-(4-(2-(perbromo-2*H*-benzo[*d*][1,2,3]triazol-2-yl)ethyl)-1*H*-1,2,3-triazol-1-yl)butanamide (5f).** The reaction of **4b** (40 mg, 0.18 mmol) with **2b** (93 mg, 0.19 mmol) afforded, after flash chromatography (Hex/AcOEt 1:5) and further hydroxamate deprotection, **5f** as a white solid (91 mg, 83%), mp 175-177 ºC. ^{1}H NMR (400 MHz, DMSO) δ 10.40 (br s, 1H), 7.86 (s, 1H), 5.07 (t, *J* = 7.2 Hz, 2H), 4.28 (t, *J* = 6.6 Hz, 2H), 3.44 (t, *J* = 7.1 Hz, 2H), 2.07-1.78 (m, 4H). ^{13}C NMR (101 MHz, DMSO) δ 168.0, 142.5, 142.3, 125.5, 122.9, 113.6, 56.4, 48.8, 28.9, 25.91, 25.7. HPLC-MS: *m/z* 632 $[M⍰H]^+$, t_R: 9.92 min, method A. Anal. calcd for $C_{14}H_{13}Br_4N_7O_2$ requires C, 26.65; H, 2.08; Br, 50.66; N, 15.54; O ,5.07; found: C, 26.84; H, 1.75; N, 15.48.

***N*-hydroxy-4-((4-(2-(perbromo-1*H*-benzo[*d*][1,2,3]triazol-1-yl)ethyl)-1*H*-1,2,3-triazol-1-yl)methyl)benzamide (5g).** The reaction of **4d** (50 mg, 0.18 mmol) with **2a** (96 mg, 0.20 mmol) afforded, after flash chromatography (DCM/MeOH 95:5) and further hydroxamate deprotection, **5g** as a white solid (87 mg, 71%), mp 139-141 ºC. ^{1}H NMR (400 MHz, DMSO) δ 11.24 (brs, 1H), 7.98 (s, 1H), 7.74 (d, *J* = 8.2 Hz, 2H), 7.26 (d, *J* = 8.2 Hz, 2H), 5.59 (s, 2H), 5.18 (t, *J* = 7.1 Hz, 2H), 3.34 (t, *J* = 7.0 Hz, 2H). ^{13}C NMR (101 MHz, DMSO) δ 164.2, 145.4, 143.1, 139.6, 133.0, 132.3, 129.1, 128.1, 127.8, 124.1, 116.3, 107.3, 52.7, 50.0, 27.5. HPLC-MS: *m/z* 680 $[M⍰H]^+$, t_R: 3.22 min, method A. Anal. calcd for $C_{18}H_{13}Br_4N_7O_2$ requires C, 31.84; H, 1.93; Br, 47.07; N, 14.44; O, 4.71; found: C, 31.71; H, 1.73; N, 14.63.

***N*-hydroxy-4-((4-(2-(perbromo-2*H*-benzo[*d*][1,2,3]triazol-2-yl)ethyl)-1*H*-1,2,3-triazol-1-yl) methyl)benzamide (5h).** The reaction of **4d** (50 mg, 0.18 mmol) with **2b** (96 mg, 0.20 mmol)

afforded, after flash chromatography (Hex/AcOEt 1:5) and further hydroxamate deprotection, **5h** as a white solid (79 mg, 65%), mp 166-168 ºC. ^{1}H NMR (400 MHz, DMSO) δ 11.21 (br s, 1H), 7.89 (s, 1H), 7.71 (d, *J* = 8.3 Hz, 2H), 7.26 (t, *J* = 8.3 Hz, 2H), 5.57 (s, 2H), 5.07 (t, *J* = 7.0 Hz, 2H), 3.45 (t, *J* = 7.0 Hz, 2H). ^{13}C NMR (101 MHz, DMSO) δ 163.6, 142.7, 142.5, 139.0, 132.4, 127.6, 127.3, 125.6, 123.3, 113.6, 56.4, 52.2, 25.7. HPLC-MS t_R: 10.33 min, non-ionizable, method A. Anal. calcd for $C_{18}H_{13}Br_4N_7O_2$ requires C, 31.84; H, 1.93; Br, 47.07; N, 14.44; O, 4.71; found: C, 31.40; H, 1.98; N, 14.35.

Molecular Modeling

On one hand, since no molecular model was available for the structure of HDAC1 at the beginning of the project, an homology model was built using SWISS MODEL web server[72-74] and was assessed by superimposition to other type I HDAC crystallized structures. The H++ web server[75] which relies on the AMBER [76] force field parameters and finite difference solutions to the Poisson-Boltzmann equation was used to calculate the protonation state of tritable groups such as the imidazole side chains of the histidine residues located in the catalytic site: His140 doubly protonated, His141 protonated in Nδ and His178 protonated in Nε. However, after all the computational work in this project was finished, a crystal structure of the complex of acetic acid-bound HDAC1 with the regulatory protein MTA1 was published under the PDB code 4BKX.[77] The amino acid sequence of the crystallized HDAC1 started at Arg8 and ended at Ala376, whereas the modelled one started at Arg8 and ended at Leu373, only three amino acids less than the crystal structure, which did not alter the overall structure of the modelled protein. Both structures were superimposed using PyMOL to assess any possible differences that would make imperative to repeat the modelling work. The overall alignment of the α-carbons of the matching amino acids presented an RMS of 0.386 Å and visual inspection of the overall structure and the binding site showed no remarkable differences that would compromise the modelled results (Supplementary Figure S7). Following these inspections we resolved not to repeat the modelling work as the results would not be substantially different. The numbering of the amino acids of the model is equivalent to the one of the crystal structure in 4BKX.

On the other hand, the structure of CK2 bound to a non-hydrolysable ATP analogue in complex with a Mg^{2+} ion (PDB code 1DAW) was used to build the kinase-bound complexes. The H++ web server predicted the side chain of His160, located at the entrance on the binding site to be doubly protonated. The missing residues and side chains were added and the macromolecule geometries refined by using Protein Preparation module in Maestro. The ligands (compounds **5c**, **5e)** were built using Maestro LigPrep module (www. Schrodinger.com). The pKa of the tritable groups were calculated using the Sparc pKa online calculator[78] and the non-protonated form of the hydroxamate was used for the docking calculations. The Glide module[79-81] was used to perform the docking calculations. For the HDAC1 complexes the centre of the box was positioned on the catalytic Zinc ion present in the active site, while for CK2 it was located at the centre of the non-hydrolysable ATP analogue of the crystal structure. The box size was set up to enclose the ligand-binding domain to ensure a proper exploration of the binding poses. The docking procedure was performed with XP (extra precision) mode, and a van der Waals radii scale factor of 1.0/0.8 for receptor and ligand, respectively. The best-obtained result for each ligand was considered for analysis of the ligand-receptor interactions and subsequent molecular modelling simulations.

For the MD simulations the charge distribution for the ligands studied was obtained by fitting the quantum mechanically calculated (RHF/6-31G**//RHF/3-21G*) molecular electrostatic potential (MEP) of the geometry-optimized molecules to a point charge model, as implemented in Gaussian 03 (Gaussian, Inc., Wallingford, CT). The general AMBER (http://ambermd.org/) force field (GAFF) was used to assign bonded and nonbonded parameters (parm03) to the ligand atoms. Each HDAC1 molecular system was immersed in a truncated octahedron containing ~10000 TIP3P water molecules[82] and 4 Cl^- ions,[83] while each CK2 system was immersed in a truncated octahedron containing ~13000 TIP3P water molecules and 9 Cl^- ions to achieve system electroneutrality. The sander and pmemd modules of the AMBER12 suite (http:// ambermd.org/) were used for the restrained and unrestrained MD simulations, respectively. Periodic boundary conditions were applied and electrostatic interactions were treated using the smooth particle mesh Ewald method[84] with a grid spacing of 1 Å. The cutoff distance for the non-bonded interactions was 9 Å, the SHAKE[85] algorithm was applied to all bonds, and an integration step of 2.0 fs was used throughout. After an initial energy minimization of the water molecules and counter-ions, the system was heated to 300 K in 25 ps after which the solvent was allowed to redistribute around the positionally restrained solute for 220 ps. After this time, they were allowed to move freely so as to explore the mutual adaptation between ligand and the protein. Snapshots from each 10-ns MD trajectory were collected every 20 ps for further analysis carried out with the ptraj module of AMBER to monitor the stability of the complexes.

Determination of CK2α inhibition

The reaction mixture (20 µL) for determination of human CK2α (prepared as described elsewhere)[86] activity contained: peptide substrate (100 µM, RRRADDSDDDDD from Aldrich), Tris-HCl pH 7.5 (20 mM), $MgCl_2$ (15 mM), 2-mercaptoethanol (6 mM) and γ[^{32}P] ATP (100 µM) and the compound (50 µM) in 5% DMSO. After 30 min of incubation at 37 ˚C, 10 µL of every assay mixture was spotted onto a square (1 cm x 1 cm) of Whatman P81 paper and dried for 15 min. Next, squares were immersed in cold 0.5% phosphoric acid, and washed 3 times, for 15 min each. Then the squares were washed with 96 % EtOH and dried for 30 min at 40˚C. The radioactivity was quantified by BECKMAN LS6500 scintillation counter. The activity was calculated as the percentage of incorporated [^{32}P]. The concentration of compound that provided 50 % inhibition of enzymatic activity (IC_{50}) was determined by semi-logarithmic dose-response plots (Graph Pad Prism 5.0 for

Windows, Graph Pad Software Inc., San Diego, California, USA, 2007).

HDAC1 inhibition assay

In vitro HDAC1 inhibition was performed using HDAC1 Fluorimetric Drug Discovery Assay Kit from *Enzo Life Sciences, Inc*. The reaction was prepared in HDAC assay buffer (50 mM Tris-HCl, pH=8.0, 137 mM NaCl, 2,7 mM KCl, 1 mM $MgCl_2$, 1 mg/mL BSA). HDAC1 enzyme (0,1 µg/well) was incubated at 37 ºC with 5 µM fluorogenic substrate at indicated concentrations of inhibitor diluted in 5% DMSO. Reactions were stopped after 60 min with the developer, and the plate was incubated at RT for 45 min, followed by measuring the fluorescence (Ex. 360nm, Em. 460nm, Synergy Mx, BioTek).

In vitro studies on mammalian cell lines

Human T-leukemia cells of Jurkat line and human breast adenocarcinoma cells of MCF-7 line were obtained from cell culture collection of Institute of Cancer Research, Vienna Medical University (Vienna, Austria). Human keratinocytes of HaCat line were obtained from Ludwig Institute for Cancer Research (Uppsala, Sweden). Murine leukemia cells of L1210 line and human embryonic kidney cells of 293T line were obtained from cell culture collection of R.E. Kavetsky Institute of Experimental Pathology, Oncology and Radiobiology, National Academy of Sciences of Ukraine (Kyiv, Ukraine). Cells were cultured in the RPMI medium supplemented with 10% fetal calf serum (Sigma Chemical Co., St. Louis, USA), 50 µg/mL streptomycin (Sigma Chemical Co., St. Louis, USA), 50 units/mL penicillin (Sigma Chemical Co., St. Louis, USA) in 5% CO_2-containing humidified atmosphere at 37 °C.

For experiments, cells were seeded into 24-well tissue culture plates (Greiner Bio-one, Germany). Stock solutions (2 mM) of each CK2 inhibitor in DMSO (99,5% pure, Sigma, USA) were prepared, and additionally dissolved in serum-free culture medium (RPMI for leukemia cells and DMEM for carcinoma cells) prior to addition to cell culture. Final concentration of DMSO in cell culture was 0,5% or less. Cytotoxicity studies on Jurkat and MCF-7 cells revealed no statistically significant toxicity of 0,5% DMSO solution on these cell lines.

Cytotoxic effect of antitumor drugs was studied under the light microscope (Evolution 300, Delta Optical, Poland) after cell staining with trypan blue dye (0.1%).

FITC-conjugated Annexin V (BD Pharmingen, USA) and propidum iodide (Sigma, USA) double staining were performed to detect early apoptotic events under treatment of Jurkat cels by CK2-HDAC inhibitors. In 24 h after the addition of **5c** and **5e** Jurkat cells were centrifuged at 2,000 rpm, washed twice with 1x PBS, and incubated for 15 min in Annexin V binding buffer (BD Pharmingen, USA) containing 1/20 volume of FITC-conjugated Annexin V solution and PI (20 PI (20 of FITC-conjugated taining1x PBS, and incubated for 15 min in Annexin V. Cytomorphological investigations were performed on Zeiss AxioImager A1 fluorescent microscope.

DAPI staining was performed for studying chromatin condensation in MCF-7 cells after treatment with **5c** and **5e**. 24 h after the addition of CK2 inhibitors, MCF-7 cells were washed twice with 1x PBS, fixed in 4 % solution of paraformaldehyde for 15 min at room temperature, and then permeabilized by 0.1% Triton X-100 solution in PBS for 3 min. Then, cells were incubated with 1 bated with 1 solution of pa,6-diamidino-2-phenylindole) (Sigma, USA) for 5 min, washed twice with PBS and cover glasses with fixed cells were placed on slides. Cytomorphological investigations were performed on Zeiss AxioImager A1 fluorescent microscope (Zeiss, Germany).

All experiments were performed in triplicate and repeated 3 times. For statistical analysis of the obtained results, standard variation data within a group was calculated together with a statistical reliability of differences between two groups of data assessed by Student alt test. The level of significance was set to 0.05.

Conclusions

We have synthesized a series of molecules that combine HDAC1 and CK2 inhibiting moieties (a hydroxamate ZBG and a TBB core, respectively) using a “click” chemistry approach. We have found dual hit compounds demonstrating excellent binding features at both target proteins. Docking and MD experiments allowed us to analyze the best linkers to connect the hydroxamate ZBG and the TBB moiety, maintaining a binding mode that resembles the one found in the previously reported crystal structures for both enzymes (Supplementary Figures S1, S4 and S5). As expected, the TBB moiety characteristic of CK2 reported inhibitors can act as a good cap group upon binging to HDAC 1. On the other hand, the widely used hydroxamate ZBG for HDAC 1 has demonstrated versatility to establish a highly effective hydrogen bonding network within the phosphate binding area in CK2. As CK2 is responsible for the regulation of HDACs by phosphorylation, we hypothesize that the combined inhibition of both enzymes in the same molecule could find clinical utility as antitumor agents. We have found compounds with similar affinity for the target proteins and cytotoxic activity in the low micromolar LC_{50} in two mammalian cancer cell lines. We consider that these new molecules are an interesting starting point for further development of antitumor drugs targeting two relevant enzymes involved in the same signaling pathway, as an attractive alternative to classical combination therapy.

section should come in this section at the end of the article, before the acknowledgements.

Acknowledgements

This work was supported by the Spanish Ministry of Science and Innovation (CTQ2011-24741 and CTQ2014-52604-R). We thank Airbus Military for fellowships to M.P. Grants to J.H.T., C.C. and K.F. from Fundación Universitaria San Pablo CEU are also acknowledged. We thank also Synthelia Organics SL. for HPLC-MS experiments.

References

1. C. L. Sawyers, *Nature*, 2007, **449**, 993-996.

2. G. R. Zimmermann, J. Lehar and C. T. Keith, *Drug Discov. Today*, 2007, **12**, 34-42.
3. E. L. Kwak, J. W. Clark and B. Chabner, *Clin. Cancer Res.*, 2007, **13**, 5232-5237.
4. S. Frantz, *Nat. Rev. Drug Discov.*, 2006, **5**, 881-882.
5. R. Morphy and Z. Rankovic, *J. Med. Chem.*, 2005, **48**, 6523-6543.
6. J. R. Morphy and C. J. Harris, *Designing multi-target drugs*, Royal Society of Chemistry, Cambridge, UK, 2012.
7. J. U. Peters, *Polypharmacology in Drug Discovery*, Wiley, Hoboken, New Jersey, Hindawi Publishing Corporation edn., 2011.
8. N. M. O'Boyle and M. J. Meegan, *Curr. Med. Chem.*, 2011, **18**, 4722-4737.
9. M. J. Fray, G. Bish, A. D. Brown, P. V. Fish, A. Stobie, F. Wakenhut and G. A. Whitlock, *Bioorg. Med. Chem. Lett.*, 2006, **16**, 4345-4348.
10. J. L. Neumeyer, X. Peng, B. I. Knapp, J. M. Bidlack, L. H. Lazarus, S. Salvadori, C. Trapella and G. Balboni, *J. Med. Chem.*, 2006, **49**, 5640-5643.
11. A. Bornot, U. Bauer, A. Brown, M. Firth, C. Hellawell and O. Engkvist, *J. Med. Chem.*, 2013, **56**, 1197-1210.
12. L. Costantino and D. Barlocco, *Curr. Med. Chem.*, 2012, **19**, 3353-3387.
13. O. Witt, H. E. Deubzer, T. Milde and I. Oehme, *Cancer Lett.*, 2009, **277**, 8-21.
14. P. A. Marks, R. A. Rifkind, V. M. Richon, R. Breslow, T. Miller and W. K. Kelly, *Nat. Rev. Cancer*, 2001, **1**, 194-202.
15. J. Graeff and L.-H. Tsai, *Annu. Rev. Pharmacol. Toxicol*, 2013, **53**, 311-330.
16. K. T. Andrews, A. Haque and M. K. Jones, *Immunol. Cell Biol.*, 2012, **90**, 66-77.
17. D. Rotili, G. Simonetti, A. Savarino, A. T. Palamara, A. R. Migliaccio and A. Mai, *Curr. Top. Med. Chem.*, 2009, **9**, 272-291.
18. P. D. Gluckman, M. A. Hanson, T. Buklijas, F. M. Low and A. S. Beedle, *Nat. Rev. Endocrinol.*, 2009, **5**, 401-408.
19. M. Haberland, R. L. Montgomery and E. N. Olson, *Nat. Rev. Genet.*, 2009, **10**, 32-42.
20. H. Lehrmann, L. L. Pritchard and A. Harel-Bellan, *Adv. Cancer Res.*, 2002, **86**, 41-65.
21. D. M. Fass, M. M. Kemp, F. A. Schroeder, F. F. Wagner, Q. Wang and E. B. Holson, Wiley-VCH-Verlag & Co. KGaA, Weinheim, Germany, 2012, pp. 515-561.
22. I. V. Gregoretti, Y. M. Lee and H. V. Goodson, *J. Mol. Biol.*, 2004, **338**, 17-31.
23. E. Pontiki and D. Hadjipavlou-Litina, *Med. Res. Rev.*, **32**, 1-165.
24. M. Paris, M. Porcelloni, M. Binaschi and D. Fattori, *J. Med. Chem.*, 2008, **51**, 1505-1529.
25. A. A. Lane and B. A. Chabner, *J. Clin. Oncol.*, 2009, **27**, 5459-5468.
26. S. Minucci and P. G. Pelicci, *Nat. Rev. Cancer*, 2006, **6**, 38-51.
27. P. A. Marks, *Oncogene*, 2007, **26**, 1351-1356.
28. C. Grant, F. Rahman, R. Piekarz, C. Peer, R. Frye, R. W. Robey, E. R. Gardner, W. D. Figg and S. E. Batest, *Expert Rev. Anticancer Ther.*, 2010, **10**, 997-1008.
29. C. Tang, C. Li, S. Zhang, Z. Hu, J. Wu, C. Dong, J. Huang and H.-B. Zhou, *J. Med. Chem.*, 2015, **58**, 4550-4572.
30. W. Duan, J. Li, E. S. Inks, C. J. Chou, Y. Jia, X. Chu, X. Li, W. Xu and Y. Zhang, *J. Med. Chem.*, 2015, **58**, 4325-4338.
31. T. Ai, H. Cui and L. Chen, *Curr. Med. Chem.*, 2012, **19**, 475-487.
32. S.-Y. Seo, *Arch. Pharmacal Res.*, 2012, **35**, 197-200.
33. W. Guerrant, V. Patil, J. C. Canzoneri and A. K. Oyelere, *J. Med. Chem.*, 2012, **55**, 1465-1477.
34. L. Chen, R. Petrelli, G. Gao, D. J. Wilson, G. T. McLean, H. N. Jayaram, Y. Y. Sham and K. W. Pankiewicz, *Bioorg. Med. Chem.*, 2010, **18**, 5950-5964.
35. L. E. Tavera-Mendoza, T. D. Quach, B. Dabbas, J. Hudon, X. Liao, A. Palijan, J. L. Gleason and J. H. White, *Proc. Natl. Acad. Sci. U. S. A.*, 2008, **105**, 8250-8255.
36. X. Cai, H.-X. Zhai, J. Wang, J. Forrester, H. Qu, L. Yin, C.-J. Lai, R. Bao and C. Qian, *J. Med. Chem.*, 2010, **53**, 2000-2009.
37. S. Mahboobi, S. Dove, A. Sellmer, M. Winkler, E. Eichhorn, H. Pongratz, T. Ciossek, T. Baer, T. Maier and T. Beckers, *J. Med. Chem.*, 2009, **52**, 2265-2279.
38. D. H. Khan, S. He, J. Yu, S. Winter, W. Cao, C. Seiser and J. R. Davie, *J. Biol. Chem.*, 2013, **288**, 16518-16528.
39. S. Pluemsampant, O. S. Safronova, K.-i. Nakahama and I. Morita, *Int. J. Cancer*, 2008, **122**, 333-341.
40. S. C. Tsai and E. Seto, *J. Biol. Chem.*, 2002, **277**, 31826-31833.
41. G. Lolli, L. A. Pinna and R. Battistutta, *ACS Chem. Biol.*, 2012, **7**, 1158-1163.
42. D. W. Litchfield, *Biochem. J*, 2003, **369**, 1-15.
43. N. A. St-Denis and D. W. Litchfield, *Cell. Mol. Life Sci.*, 2009, **66**, 1817-1829.
44. K. A. Ahmad, G. Wang, G. Unger, J. Slaton and K. Ahmed, in *Advances in Enzyme Regulation, Vol 48*, eds. G. Weber, C. E. ForrestWeber and L. Cocco, 2008, vol. 48, pp. 179-187.
45. B. Guerra and O.-G. Issinger, *Curr. Med. Chem.*, 2008, **15**, 1870-1886.
46. G. M. Unger, A. T. Davis, J. W. Slaton and K. Ahmed, *Curr. Cancer Drug Targets*, 2004, **4**, 77-84.
47. G. Cozza, L. A. Pinna and S. Moro, *Curr. Med. Chem.*, 2013, **20**, 671-693.
48. G. Cozza, C. Girardi, A. Ranchio, G. Lolli, S. Sarno, A. Orzeszko, Z. Kazimierczuk, R. Battistutta, M. Ruzzene and L. A. Pinna, *Cell. Mol. Life Sci.*, 2014, **71**, 3173-3185.
49. R. Battistutta, *Cell. Mol. Life Sci.*, 2009, **66**, 1868-1889.
50. S. Sarno, S. Moro, F. Meggio, G. Zagotto, D. Dal Ben, P. Ghisellini, R. Battistutta, G. Zanotti and L. A. Pinna, *Pharmacol. Ther.*, 2002, **93**, 159-168.
51. J. Raaf, B. Guerra, I. Neundorf, B. Bopp, O.-G. Issinger, J. Jose, M. Pietsch and K. Niefind, *ACS Chem. Biol.*, 2013, **8**, 901-907.
52. R. Prudent and C. Cochet, *Chem. Biol.*, 2009, **16**, 112-120.
53. F. Pierre, P. C. Chua, S. E. O'Brien, A. Siddiqui-Jain, P. Bourbon, M. Haddach, J. Michaux, J. Nagasawa, M. K. Schwaebe, E. Stefan, A. Vialettes, J. P. Whitten, T. K. Chen, L. Darjania, R. Stansfield, K. Anderes, J. Bliesath, D. Drygin, C. Ho, M. Omori, C. Proffitt, N. Streiner, K. Trent, W. G. Rice and D. M. Ryckman, *J. Med. Chem.*, 2011, **54**, 635-654.
54. R. Battistutta, G. Cozza, F. Pierre, E. Papinutto, G. Lolli, S. Sarno, S. E. O'Brien, A. Siddiqui-Jain, M. Haddach, K. Anderes, D. M. Ryckman, F. Meggio and L. A. Pinna, *Biochemistry*, 2011, **50**, 8478-8488.
55. R. Swider, M. Maslyk, J. M. Zapico, C. Coderch, R. Panchuk, N. Skorokhyd, A. Schnitzler, K. Niefind, B. de

Pascual-Teresa and A. Ramos, *Rsc Advances*, 2015, **5**, 72482-72494.
56. P. Thirumurugan, D. Matosiuk and K. Jozwiak, *Chem. Rev.*, 2013, **113**, 4905-4979.
57. M. A. Pagano, M. Andrzejewska, M. Ruzzene, S. Sarno, L. Cesaro, J. Bain, M. Elliott, F. Meggio, Z. Kazimierczuk and L. A. Pinna, *J. Med. Chem.*, 2004, **47**, 6239-6247.
58. R. Swider, M. Maslyk, S. Martin-Santamaria, A. Ramos and B. de Pascual-Teresa, *Mol. Cell. Biochem.*, 2011, **356**, 117-119.
59. J. M. Zapico, P. Serra, J. Garcia-Sanmartin, K. Filipiak, R. J. Carbajo, A. K. Schott, A. Pineda-Lucena, A. Martinez, S. Martin-Santamaria, B. de Pascual-Teresa and A. Ramos, *Org. Biomol. Chem.*, 2011, **9**, 4587-4599.
60. A. L. Edinger and C. B. Thompson, *Curr. Opin. Cell Biol.*, 2004, **16**, 663-669.
61. I. Vermes, C. Haanen, H. Steffensnakken and C. Reutelingsperger, *J. Immunol. Methods*, 1995, **184**, 39-51.
62. A. Vannini, C. Volpari, P. Gallinari, P. Jones, M. Mattu, A. Carfi, R. De Francesco, C. Steinkuehler and S. Di Marco, *EMBO Rep.*, 2007, **8**, 879-884.
63. J. R. Somoza, R. J. Skene, B. A. Katz, C. Mol, J. D. Ho, A. J. Jennings, C. Luong, A. Arvai, J. J. Buggy, E. Chi, J. Tang, B. C. Sang, E. Verner, R. Wynands, E. M. Leahy, D. R. Dougan, G. Snell, M. Navre, M. W. Knuth, R. V. Swanson, D. E. McRee and L. W. Tari, *Structure*, 2004, **12**, 1325-1334.
64. D. P. Dowling, S. L. Gantt, S. G. Gattis, C. A. Fierke and D. W. Christianson, *Biochemistry*, 2008, **47**, 13554-13563.
65. K. Vanommeslaeghe, C. Van Alsenoy, F. De Proft, J. C. Martins, D. Tourwe and P. Geerlings, *Org. Biomol. Chem.*, 2003, **1**, 2951-2957.
66. K. Niefind, M. Putter, B. Guerra, O. G. Issinger and D. Schomburg, *Nat. Struct. Biol.*, 1999, **6**, 1100-1103.
67. R. Battistutta, E. De Moliner, S. Sarno, G. Zanotti and L. A. Pinna, *Protein Sci.*, 2001, **10**, 2200-2206.
68. R. Battistutta, M. Mazzorana, L. Cendron, A. Bortolato, S. Sarno, Z. Kazimierczuk, G. Zanotti, S. Moro and L. A. Pinna, *Chembiochem*, 2007, **8**, 1804-1809.
69. R. Szyszka, N. Grankowski, K. Felczak and D. Shugar, *Biochem. Biophys. Res. Commun.*, 1995, **208**, 418-424.
70. Y. Zhou, S. Wang, K. Zhang and X. Jiang, *Angew. Chem. Int. Ed.*, 2008, **47**, 7454-7456.
71. K. Barral, A. D. Moorhouse and J. E. Moses, *Org. Lett.*, 2007, **9**, 1809-1811.
72. M. C. Peitsch, *Bio-Technology*, 1995, **13**, 723-723.
73. F. Kiefer, K. Arnold, M. Kuenzli, L. Bordoli and T. Schwede, *Nucleic Acids Res.*, 2009, **37**, D387-D392.
74. K. Arnold, L. Bordoli, J. Kopp and T. Schwede, *Bioinformatics*, 2006, **22**, 195-201.
75. J. C. Gordon, J. B. Myers, T. Folta, V. Shoja, L. S. Heath and A. Onufriev, *Nucleic Acids Res.*, 2005, **33**, W368-W371.
76. W. D. Cornell, P. Cieplak, C. I. Bayly, I. R. Gould, K. M. Merz, D. M. Ferguson, D. C. Spellmeyer, T. Fox, J. W. Caldwell and P. A. Kollman, *J. Am. Chem. Soc.*, 1995, **117**, 5179-5197.
77. C. J. Millard, P. J. Watson, I. Celardo, Y. Gordiyenko, S. M. Cowley, C. V. Robinson, L. Fairall and J. W. Schwabe, *Mol. Cell*, 2013, **51**, 57-67.
78. S. H. Hilal, S. W. Karickhoff and L. A. Carreira, *Quant. Struct.-Act. Relat.*, 1995, **14**, 348-355.
79. R. A. Friesner, R. B. Murphy, M. P. Repasky, L. L. Frye, J. R. Greenwood, T. A. Halgren, P. C. Sanschagrin and D. T. Mainz, *J. Med. Chem.*, 2006, **49**, 6177-6196.
80. T. A. Halgren, R. B. Murphy, R. A. Friesner, H. S. Beard, L. L. Frye, W. T. Pollard and J. L. Banks, *J. Med. Chem.*, 2004, **47**, 1750-1759.
81. R. A. Friesner, J. L. Banks, R. B. Murphy, T. A. Halgren, J. J. Klicic, D. T. Mainz, M. P. Repasky, E. H. Knoll, M. Shelley, J. K. Perry, D. E. Shaw, P. Francis and P. S. Shenkin, *J. Med. Chem.*, 2004, **47**, 1739-1749.
82. W. L. Jorgensen, J. Chandrasekhar, J. D. Madura, R. W. Impey and M. L. Klein, *J. Chem. Phys.*, 1983, **79**, 926-935.
83. J. Aqvist, *J. Phys. Chem.*, 1990, **94**, 8021-8024.
84. C. Hansch, *J. Comput. Aided Mol. Des.*, 2011, **25**, 495-507.
85. M. A. Lill, *Biochemistry*, 2011, **50**, 6157-6169.
86. T. Fraczyk, K. Kubinski, M. Maslyk, J. Ciesla, U. Hellman, D. Shugar and W. Rode, *Bioorg. Chem.*, 2010, **38**, 124-131.